First-Principles Materials Design of High-Performing Bulk Photovoltaics with the $LiNbO_3$ Structure

Steve M. Young

Center for Computational Materials Science, United States Naval Research Laboratory, Washington, DC 20375, USA

Fan Zheng and Andrew M. Rappe

Department of Chemistry, The Makineni Theoretical Laboratories, University of Pennsylvania, Philadelphia, Pennsylvania 19104-6323, USA

(Received 24 August 2015; published 18 November 2015)

The bulk photovoltaic effect is a long-known but poorly understood phenomenon. Recently, however, the multiferroic bismuth ferrite has been observed to produce strong photovoltaic response to visible light, suggesting that the effect has been underexploited. Here we present three polar oxides in the $LiNbO_3$ structure that we predict to have band gaps in the 1–2 eV range and very high bulk photovoltaic response: $PbNiO_3$, $Mg_{1/2}Zn_{1/2}PbO_3$, and $LiBiO_3$. All three have band gaps determined by cations with $d^{10}s^0$ electronic configurations, leading to conduction bands composed of cation s orbitals and O p orbitals. This both dramatically lowers the band gap and increases the bulk photovoltaic response by as much as an order of magnitude over previous materials, demonstrating the potential for high-performing bulk photovoltaics.

DOI: 10.1103/PhysRevApplied.4.054004

I. INTRODUCTION

Photovoltaic effects have long been observed in bulk polar materials, especially ferroelectrics [1–4]. Known as the bulk photovoltaic effect (BPVE), it appeared to derive from inversion symmetry breaking. Despite intense initial interest, early explorations revealed low energy-conversion efficiency, in part due to the high band gaps of most known ferroelectrics. Additionally, despite several proposed mechanisms, the physical origin of the BPVE was unclear [2,5–8].

However, the recent emphasis on alternative energy technologies and the observation of the effect in novel semiconducting ferroelectrics (with band gaps in the visible range) has renewed interest [9–15]. Several studies have attempted to elucidate the various contributions to the photovoltaic response—bulk or otherwise—in ferroelectrics [16–24]. In particular, bismuth ferrite ($BiFeO_3$) has been found to generate significant bulk photocurrents; combined with its unusually low band gap of 2.7 eV, it has attracted a great deal of attention for its potential in photovoltaic applications [22,24–32]. The understanding of the fundamental physics behind the effect has advanced as well; recently, we demonstrated that the BPVE can be attributed to "shift currents," and that the bulk photocurrents may be calculated from first principles [33,34]. The *ab initio* calculation of the shift current and subsequent analysis yielded several chemical and structural criteria for optimizing the response. These criteria have been used previously to modify or identify existing materials with enhanced response [14,35–37]. In this work, we use these insights to propose several candidate bulk photovoltaics with calculated response as much as an order of magnitude higher than well-known ferroelectrics, while having band gaps in or slightly below the visible spectrum. Our results demonstrate that the bulk photovoltaic response can be much stronger than previously observed, supporting the possibility of materials suitable for application.

II. OVERVIEW OF SHIFT CURRENT BPVE

There are two figures of merit for evaluating the BPVE in a material: the current-density response to a spatially uniform electric field, and the Glass coefficient [3]. The current-density response is given by the tensor

$$J_q(\omega) = \sigma_{rsq}(\omega)E_r^0(\omega)E_s^0(\omega),$$
$$\sigma_{rsq}(\omega) = e\sum_{n',n''}\int d\mathbf{k}\mathcal{I}_{rs}(n',n'',\mathbf{k};\omega)\mathcal{R}_q(n',n'',\mathbf{k}),$$

where $\mathbf{E}^0$ is the vector of the illumination field, and n' and n'' index bands. Letting f denote filling, χ the Berry connection, and ϕ the phase of the transition dipole, the expression

$$\mathcal{I}_{rs}(n',n'',\mathbf{k};\omega) = \pi\left(\frac{e}{m\hbar\omega}\right)^2(f[n''\mathbf{k}]-f[n'\mathbf{k}]) \times\langle n'\mathbf{k}|\hat{P}_r|n''\mathbf{k}\rangle\langle n''\mathbf{k}|\hat{P}_s|n'\mathbf{k}\rangle \times\delta(\omega_{n''}(\mathbf{k})-\omega_{n'}(\mathbf{k})\pm\omega) \quad (1)$$

describes the intensity of transitions, and

$$\mathcal{R}_q(n',n'',\mathbf{k}) = -\frac{\partial\phi_{n'n''}(\mathbf{k},\mathbf{k})}{\partial k_q} - [\chi_{n''q}(\mathbf{k})-\chi_{n'q}(\mathbf{k})] \quad (2)$$

is the expression for the "shift vector," which describes a distance associated with the excited carrier [5,38], and depends on the differences in the wave-function centers up to a unit cell, as provided by the Berry connections, and the average separation in unit cells given by the transition dipole phase derivative. Roughly speaking, the two terms $\mathcal{I}$ and $\mathcal{R}$ can be thought of as giving the number of carriers excited and the velocity of those carriers. We emphasize that this mechanism is profoundly different from other photovoltaic effects; rather than relying on the excitation of carriers which are then separated by an electric field, the carriers are electrons (holes) in coherent excited states that possess intrinsic momentum of opposite sign. Crucially, this allows for arbitrarily high photovoltages; the Shockley-Queisser limit does not apply, a major advantage of BPVE. In particular, the open-circuit voltage is determined by the competition between the photocurrent and countervailing voltage-driven leakage that depends on the overall resistance of the sample [39]. This sample dependence prevents straightforward calculation of open-circuit voltages and ultimate efficiencies.

Determining the total current in a sample is complicated by the attenuation of incident illumination as it travels through the material. In the limit of a thick sample that will completely absorb the illumination, the total current can be obtained from the Glass coefficient G

$$\bar{J}_q(\omega) = \frac{\sigma_{rrq}(\omega)}{\alpha_{rr}(\omega)} |E_r^0(\omega)|^2 \mathcal{W} = G_{rrq}(\omega) I_r(\omega) \mathcal{W}, \quad (3)$$

where α is the absorption coefficient and $\mathcal{W}$ is the sample width. Thus, the current-density tensor and Glass coefficient describe the response in the regimes of near-zero and near-infinite thickness, respectively. In practice, "infinite thickness" is on the order of microns, and total photocurrent is usually best described by the Glass coefficient.

However, the Glass coefficient provides additional information about the response. In the limit where $\epsilon^i \ll \epsilon^r$,

$$\alpha \approx \frac{\omega}{cn}\epsilon^i = \left(\frac{e}{m}\right)^2 \frac{\pi}{\epsilon_0 cn\hbar\omega} \sum_{n',n''} \int d\mathbf{k} \mathcal{I}_{rs}(n', n'', \mathbf{k}; \omega)$$

and the Glass coefficient becomes

$$G_{rrq}(\omega) = \frac{1}{2\epsilon_0 cn} \frac{\sigma_{rrq}(\omega)}{\alpha_{rr}(\omega)} = \frac{e}{2\hbar\omega} \frac{\sum_{n',n''} \int d\mathbf{k} \mathcal{I}_{rr}(n', n'', \mathbf{k}; \omega) R_q(n', n'', \mathbf{k})}{\sum_{n'n''} \int d\mathbf{k} \mathcal{I}_{rr}(n', n'', \mathbf{k}; \omega)}.$$

The Glass coefficient is therefore closely related to the weighted average shift vector, allowing us to estimate the contribution of both terms in the shift-current expression.

III. METHODS

The shift-current response is calculated as in Ref. [33], from wave functions generated using density functional theory, with the generalized-gradient approximation (GGA) and optimized, norm-conserving pseudopotentials [40,41]. The presented results exclude spin-orbit effects; calculations with and without spin orbit were performed for both $LiBiO_3$ and $Mg_{1/2}Zn_{1/2}PbO_3$, and were not found to substantially influence the results. For $BiFeO_3$, a Hubbard U of 5 eV is used for Fe $3d$, as in Ref. [34]. For $PbNiO_3$, a Hubbard U of 4.6 eV is used for Ni $3d$, as in Ref. [42]. QUANTUM ESPRESSO [43] is used for the electronic structure calculations, and OPIUM is used to generate pseudopotentials. The Heyd-Scuseria-Ernzerhof (HSE) hybrid functional [44] is used to compute band gaps, as it is known to frequently produce significantly more accurate values than GGA. These calculations are performed on $8 \times 8 \times 8$ k-point grids, with $4 \times 4 \times 4$ grids for the exact-exchange HSE calculations. Band structures and density-of-states plots are generated from GGA calculations, and reported HSE band gaps are the direct gaps. The present results are for the experimental structure in the cases of $BiFeO_3$ and $PbNiO_3$, and computationally relaxed structures for the other materials. Structural relaxations and calculations of shift current were performed at the level of the local-density approximation and found to vary minimally from the GGA results; due to the high expense of exact-exchange calculations, the dense k-point grids required to converge shift-current calculations cannot presently be obtained using HSE, and scissor corrections [45,46] to the HSE gaps are applied to account for the dependence of the Glass coefficient on frequency.

IV. MATERIALS DESIGN APPROACH

Previously, we revealed the dependence of shift-vector magnitude on the chemical and structural properties of materials. Large shift vectors are characterized by valence and/or conduction states that are both strongly asymmetric and delocalized in the current direction [33]. In this regard, many distorted perovskite (ABO_3) ferroelectrics are crippled by the presence of d^0 cations enclosed in octahedral oxygen cages. The conduction-band edge is dominated by t_{2g}-like d states that are largely nonbonding. Coupled with the tendency for d states to localize, the result is that both shift vectors and transition response are very weak near the band gap. The delocalized e_g states are much higher in energy, effectively raising the energy threshold for significant BPVE.

To overcome the weak BPVE response of d^0 oxides, we investigated systems that involve both large distortions to oxygen cages (increasing the bonding character of any d^0 states) as well as d^{10} cations with less localized s and/or p states near the band edge [35]. It has already been noted that d^{10} cations can dramatically improve the activity of

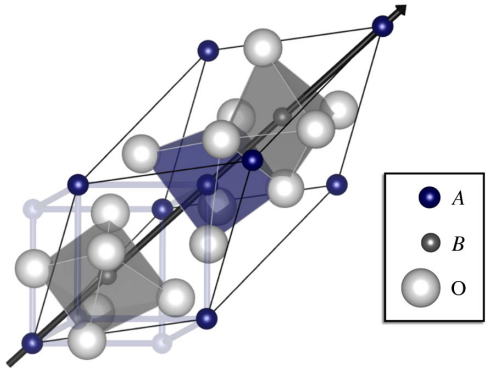

FIG. 1. The $LiNbO_3$ primitive cell, overlaid with the pseudocubic perovskite cell. The direction of the polar distortion is indicated by the black arrow. Image created using the VESTA visualization program [55].

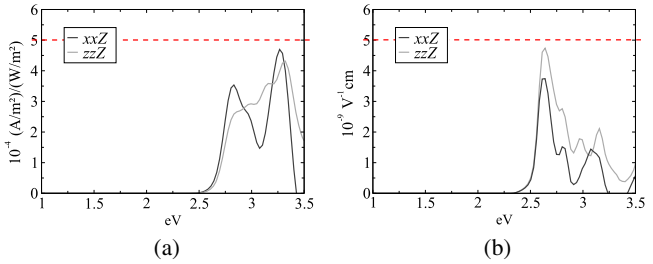

FIG. 2. The current-density response for $BiFeO_3$ (GGA + U) is shown in (a). The Glass coefficient of $BiFeO_3$ appears in (b). Only the response in the direction of material polarization is shown, for both perpendicular (xxZ) and parallel (zzZ) light polarization. Dashed lines appear at benchmark values of current density and Glass coefficient chosen to represent the maximum response of these materials.

photocatalysts [47]. We found polar oxides taking the $LiNbO_3$ structure to be promising candidates, with $d^{10}s^0$ cations Pb^{4+} and Bi^{5+}. This structure can also be obtained by distorting the perovskite structure rhombohedrally, and allowing polar distortions along and oxygen-cage rotations about $\langle 111 \rangle$. Notable ferroelectrics with this structure (but with d^0 cations) include $LiNbO_3$ and $BiFeO_3$. $LiNbO_3$ is known for its large nonlinear optical response, and, often doped with iron, it was one of the first materials in which the bulk photovoltaic effect was observed and studied [2,48,49]. However, its bulk band gap is well outside the visible spectrum [50]. $BiFeO_3$ has garnered much attention recently for its multiferroic behavior [51] and low band gap of about 2.74 eV [52], which has led to explorations of its photovoltaic response [22–25,53,54]. We have used $BiFeO_3$ as a benchmark for the present study; as with the archetypal ferroelectrics $BaTiO_3$ and $PbTiO_3$, its LUMO is dominated by cation d states and yields a very similar response magnitude.

We consider only the current response in the direction of material polarization for both perpendicular (xxZ) and parallel (zzZ) light polarization, as these are the only tensor elements that can contribute to the response to unpolarized light. For ease of comparison, we mark baseline values reflecting the maximum in the calculated frequency-dependent responses of $BiFeO_3$ within the visible spectrum, shown in Fig. 1, with a dashed, red line. These are, for the current density and Glass coefficient, respectively, 5×10^{-4} $(A/m^2)/(W/m^2)$ and 5×10^{-9} cm/V.

We have studied three materials taking the $LiNbO_3$ structure (Fig. 2): $PbNiO_3$, $Mg_{1/2}Zn_{1/2}PbO_3$, and $LiBiO_3$. The first has been synthesized [56], and the latter two are similar in composition to known materials. The structural parameters and bulk polarizations are given in Table I. The distortion from cubic perovskite is sufficiently strong that assignment of A sites and B sites is ambiguous. We have followed the assignment of Ref. [56] for $PbNiO_3$, but note that treating Ni as the A site (reversing the orientation), the Wyckoff position of oxygen becomes (0.800, 0.116, 0.384), which is slightly closer to the corresponding crystal coordinate of the other two materials. All three satisfy our requirements of low band gap, d^{10} cations, and large polar distortions. Furthermore, as seen in Fig. 3, all three have qualitatively similar band structures, featuring highly dispersive conduction bands, in contrast to the usual case of d^0 perovskite derivatives. As we will show, this arises due to unfilled s-like—rather than d-like—states composing the conduction band, and has profound consequences for the bulk photovoltaic response.

TABLE I. The structural data for the three compounds presented here. $PbNiO_3$ and $LiBiO_3$ are in space group $R3c$, while $Mg_{1/2}Zn_{1/2}PbO_3$ is in $R3$. However, the deviations of the coordinates from the $R3c$ positions are minuscule ($< 0.2\%$), so they are presented as such with Mg and Zn each occupying one site of the A position. Polarizations are determined based on a nonpolar structure featuring the A-site atom coplanar with oxygen, and the B-site midway between oxygen planes [57–60].

	$PbNiO_3$	$Mg_{1/2}Zn_{1/2}PbO_3$	$LiBiO_3$
a	5.63 Å	5.77 Å	5.67 Å
α	57°	57°	56°
A (2a)	(0.0, 0.0, 0.0)	(0.0, 0.0, 0.0)	(0.0, 0.0, 0.0)
B (2a)	(0.214, 0.214, 0.214)	(0.216, 0.216, 0.216)	(0.213, 0.213, 0.213)
O (6b)	(0.830, 0.098, 0.415)	(0.794, 0.128, 0.390)	(0.798, 0.122, 0.405)
P	99 $\mu C/cm^2$	83 $\mu C/cm^2$	50 $\mu C/cm^2$

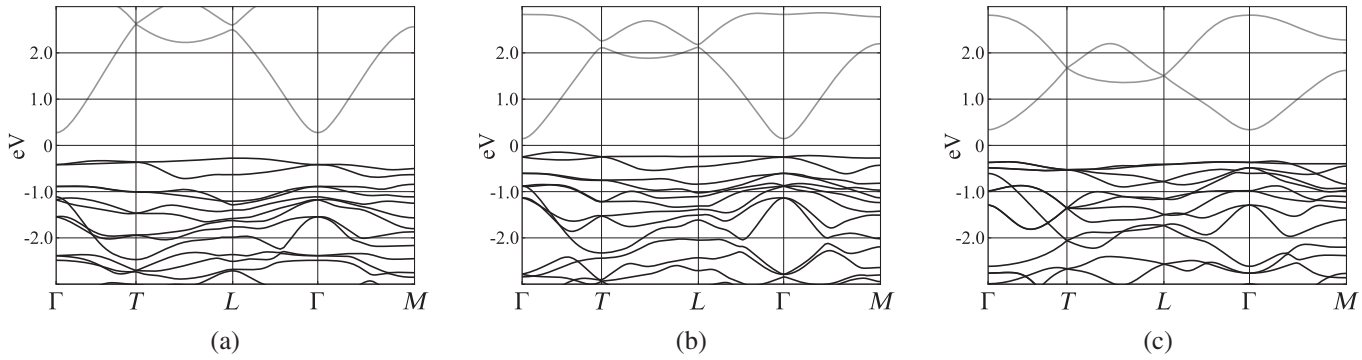

FIG. 3. The band structures of (a) $PbNiO_3$, (b) $Mg_{1/2}Zn_{1/2}PbO_3$, and (c) $LiBiO_3$. Note the similar, highly dispersive conduction-band edges.

V. $PbNiO_3$

$PbNiO_3$ has recently been synthesized [56] and explored theoretically [42,61]. Like $BiFeO_3$, it is antiferromagnetic with a weak spin canting, and possesses an even larger polarization, calculated at 100 $\mu C/cm^2$ [42]. Its band gap is even lower than $BiFeO_3$, with HSE predicting 1.2 eV [42]. In $BiFeO_3$, Bi has the oxidation state 3+, so that its 6*s* orbital is filled, and the exchange splitting of Fe determines the gap. However, in $PbNiO_3$, Pb is 4+, and its 6*s* states appear lower in energy than the Ni exchange-split bands, resulting in a distinct electronic profile. This can be clearly seen in the projected density of states [Fig. 4(a)]: the lowest conduction band is almost entirely Pb 6*s* and O 2*p* states, while the *d* states only appear in the valence band and higher in the conduction manifold. While this serves to lower the band gap dramatically, a further result of this is a Glass coefficient [Fig. 4(d)] over an order of magnitude larger than the benchmark value. The current density is modest by comparison, though it still exceeds the benchmark, indicating large shift vectors with relatively low absorption.

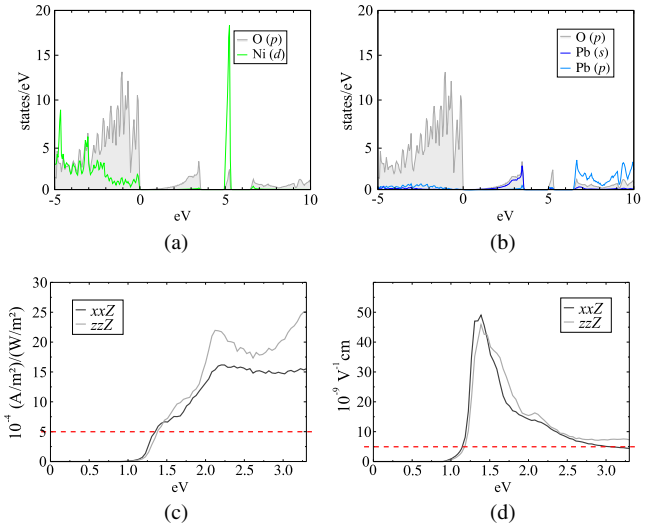

FIG. 4. (a) and (b) give the projected density of states for $PbNiO_3$. The unfilled half of e_g of the high-spin d^8 Ni appears as a sharp peak *above* the unfilled Pb *s* orbitals, which have strongly hybridized with oxygen *p* orbitals, resulting in a low band gap (1.2 eV in HSE [42]). This material has a large (c) current-density response (≈4 × benchmark), and a very large (d) Glass coefficient (≈10 × benchmark).

VI. $Mg_{1/2}Zn_{1/2}PbO_3$

$HgPbO_3$ [62] and $ZnSnO_3$ [63,64] are known to take the ilmenite and $LiNbO_3$ structures, respectively. However, the first is metallic and the second has a high band gap and only modest photovoltaic response. We first calculated the response of $ZnPbO_3$, but found it to be borderline metallic, despite a promising response; to raise the gap, we substituted Mg for half of the Zn. Phonon calculations indicate that the structure is metastable. Once again, as seen

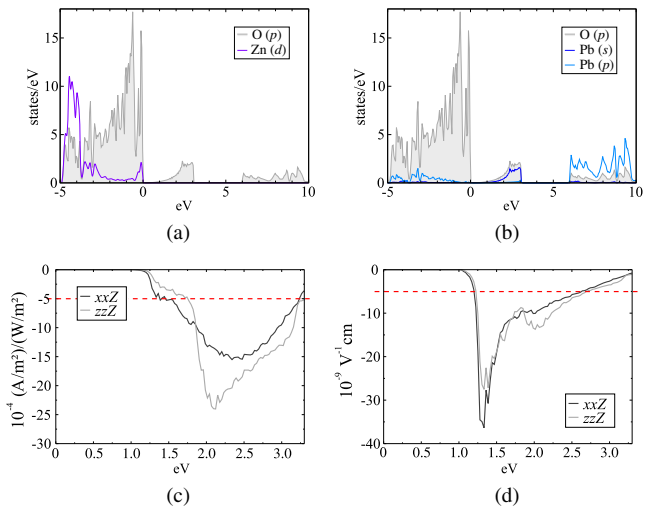

FIG. 5. Orbital-projected densities of states for $Mg_{1/2}Zn_{1/2}PbO_3$ are shown in (a) and (b). The valence band is formed almost entirely from oxygen *p* orbitals, and the conduction band is hybridized Pb 6*s* and O 2*p* states. This results in a low band gap (1.2 in HSE), (c) a high current-density response (≈4 × benchmark), and (d) a very large Glass coefficient (≈7 × benchmark).

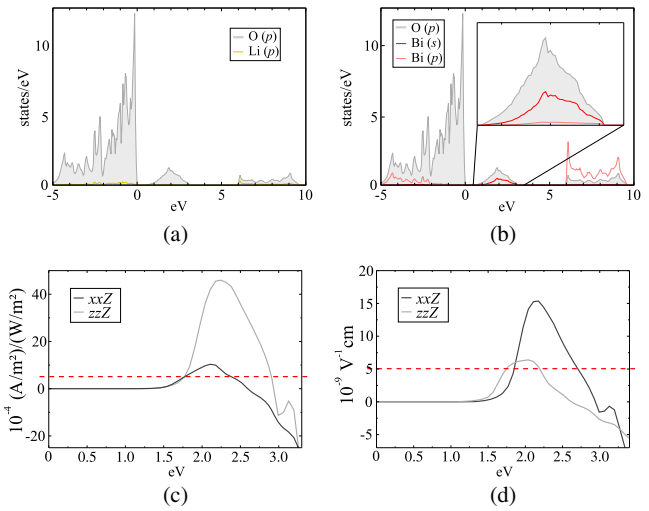

FIG. 6. The density of states for $LiBiO_3$, shown in (a) and (b), is dominated by bismuth and oxygen. The band gap is set by transitions from O $2p$ to hybridized Bi $6s$ states. The band gap is modest (1.7 eV in HSE). The current-density response shown in (c) is quite high ($\approx 8\times$ benchmark), with a large (d) Glass coefficient ($\approx 3\times$ benchmark), indicating strong absorption in addition to long shift vectors.

in Fig. 5(b), hybridized Pb $6s$ states compose the lowest unfilled band. The magnitude of the response is quite high, but the current is antiparallel to the computed polarization. This is unlike most materials, including our benchmark materials and the aforementioned $PbNiO_3$, however, we emphasize the ambiguity of both polarization (the addition of polarization quanta) and structure orientation (designation of A and B cations) for these materials. If we compare the two Pb compounds with Pb as the B site in both, not only are the structures more similar, but their responses become parallel.

VII. $LiBiO_3$

$LiBiO_3$ is known to exist in a structure with edge sharing oxygen octahedra [65]. However, our calculations place the $LiNbO_3$-type structure—which phonon analysis reveals to be metastable—nearby in energy, at only about 0.01 eV per atom higher; additionally, $NaBiO_3$ is known to take the closely related ilmenite structure [65]. In light of this, we consider it highly possible that the $LiBiO_3$ can be synthesized in the $LiNbO_3$ structure.

As shown in Figs. 6(a) and 6(b), the electronic structure is very similar to the previous two materials. As with Pb-containing compounds, the low-lying hybridized Bi s states form the lowest unfilled bands, though the Bi s proportion is lower than that of Pb s in the aforementioned materials. Possibly as a consequence, the dispersion of the conduction band is reduced compared to $PbNiO_3$ and $Mg_{1/2}Zn_{1/2}PbO_3$ (Fig. 3), and the BPVE response is somewhat different: while the Glass coefficient is not as large as for the two lead-containing materials, the photocurrent density is higher, indicating increased absorption. Additionally, the band gap is larger, with HSE predicting 1.7–1.8 eV, positioned almost perfectly with respect to the visible spectrum for solar energy conversion.

It is worth contrasting the response of $LiBiO_3$ with that of the two lead compounds: the former has a notably distinct response, especially near the band edge. This can be attributed to the difference in the valence band character; in $PbNiO_3$ and $Mg_{1/2}Zn_{1/2}PbO_3$ the valence band edge contains considerable density from the secondary cation's filled d states. This alters the character of the wave functions and improves delocalization and response magnitude by sharing density, as opposed to lithium's almost completely ionic character. This suggests that inclusion of an appropriate dopant with higher electronegativity may allow for significant tuning of the response in $LiBiO_3$.

VIII. CONCLUSION

We have proposed several polar oxides in the $LiNbO_3$ structure with a strong computed BPVE response and low band gaps, summarized in Table II. The compositions, featuring Pb^{4+} or Bi^{5+} cations, are chosen for the absence of d states at the band edge. Instead, these materials have conduction bands formed by low-lying s states hybridized with oxygen p states. In addition to creating significantly lower band gaps, this makes for large, diffuse orbitals and strongly delocalized states; combined with large polar distortions, they effect a significant shift-current response that is over an order of magnitude higher than that previously observed, and roughly double the best performing materials previously proposed. Given the minimal contributions from the other cations, the possibility of tuning the response via composition without altering its fundamental character is strongly suggested. Moreover, in combination with recent demonstrations that careful device construction can dramatically improve BPVE device performance [13,24,39], these results indicate that BPVE can

TABLE II. The band gap and response characteristics of the presented materials, along with benchmark $BiFeO_3$ and other recently proposed bulk photovoltaics (with scissor corrected responses) for comparison.

	Direct gap	Maximum G	Maximum σ
	eV	$\times 10^{-9}$ cm/V	$\times 10^{-4}$ $[(A/m^2)/(W/m^2)]$
$BiFeO_3$	2.7 [52]	5	5
KBNNO [37]	1.3 (HSE)	25	5
$LiAsSe_2$ [36]	1.1 [66]	30	98
$PbNiO_3$	1.2 (HSE) [42]	50	25
$Mg_{1/2}Zn_{1/2}PbO_3$	1.2 (HSE)	35	25
$LiBiO_3$	1.7 (HSE)	15	45

be much stronger than previously thought, bolstering hopes that the phenomenon can be successfully exploited.

S. M. Y. was supported by the Department of Energy Office of Basic Energy Sciences, under Grant No. DE-FG02-07ER46431, and by the U.S. Naval Research Laboratory through the National Research Council Research Associateship Program. F. Z. was supported by the Office of Naval Research under Grant No. N00014-14-1-0761. A. M. R was supported by the Office of Naval Research under Grant No. N00014-12-1-1033. Computational support was provided by the HPCMO of the DoD and NERSC of the DOE.

[1] A. G. Chynoweth, Surface space-charge layers in barium titanate, Phys. Rev. **102**, 705 (1956).
[2] F. S. Chen, Optically induced change of refractive indices in $LiNbO_3$ and $LiTaO_3$, J. Appl. Phys. **40**, 3389 (1969).
[3] A. M. Glass, D. von der Linde, and T. J. Negran, High-voltage bulk photovoltaic effect and photorefractive process in $LiNbO_3$, Appl. Phys. Lett. **25**, 233 (1974).
[4] V. M. Fridkin, Bulk photovoltaic effect in noncentrosymmetric crystals, Crystallogr. Rep. (Transl. Kristallografiya) **46**, 654 (2001).
[5] R. von Baltz and W. Kraut, Theory of the bulk photovoltaic effect in pure crystals, Phys. Rev. B **23**, 5590 (1981).
[6] Boris I. Sturman and Vladimir M. Fridkin, *The Photovoltaic and Photorefractive Effects in Noncentrosymmetric Materials*, edited by George W. Taylor, series Ferroelectricity and Related Phenomena Vol. 8 (Gordon and Breach Science Publishers, Philadelphia, 1992).
[7] F. Jermann and J. Otten, Light-induced charge-transport in $LiNbO_3$: Fe at high light intensities, J. Opt. Soc. Am. B **10**, 2085 (1993).
[8] Kazuhiko Tonooka, Patcharin Poosanaas, and Kenji Uchino, *Mechanism of the Bulk Photovoltaic Effect in Ferroelectrics* (International Society for Optics and Photonics, San Diego, 1994), pp. 224–232.
[9] Ilya Grinberg, D. Vincent West, Maria Torres, Gaoyang Gou, David M. Stein, Liyan Wu, Guannan Chen, Eric M. Gallo, Andrew R. Akbashev, Peter K. Davies, Jonathan E. Spanier, and Andrew M. Rappe, Perovskite oxides for visible-light-absorbing ferroelectric and photovoltaic materials, Nature (London) **503**, 509 (2013).
[10] Ratheesh K. Vijayaraghavan, Stefan C. J. Meskers, M. Abdul Rahim, and Suresh Das, Bulk photovoltaic effect in an organic polar crystal, Chem. Commun. **50**, 6530 (2014).
[11] C. Somma, K. Reimann, C. Flytzanis, T. Elsaesser, and M. Woerner, High-Field Terahertz Bulk Photovoltaic Effect in Lithium Niobate, Phys. Rev. Lett. **112**, 146602 (2014).
[12] Marco M. Furchi, Andreas Pospischil, Florian Libisch, Joachim Burgdörfer, and Thomas Mueller, Photovoltaic effect in an electrically tunable van der Waals heterojunction, Nano Lett. **14**, 4785 (2014).
[13] A. Zenkevich, Yu. Matveyev, K. Maksimova, R. Gaynutdinov, A. Tolstikhina, and V. Fridkin, Giant bulk photovoltaic effect in thin ferroelectric $BaTiO_3$ films, Phys. Rev. B **90**, 161409 (2014).
[14] Fan Zheng, Hiroyuki Takenaka, Fenggong Wang, Nathan Z. Koocher, and Andrew M. Rappe, First-principles calculation of the bulk photovoltaic effect in $CH_3NH_3PbI_3$ and $CH_3NH_3PbI_{3-x}Cl_x$, J. Phys. Chem. Lett. **6**, 31 (2015).
[15] B. Kolb and A. M. Kolpak, First-principles design and analysis of an efficient, Pb-free ferroelectric photovoltaic absorber derived from $ZnSnO_3$, Chem. Mater. **27**, 5899 (2015).
[16] M. Ichiki, H. Furue, T. Kobayashi, R. Maeda, Y. Morikawa, T. Nakada, and K. Nonaka, Photovoltaic properties of $(Pb, La)(Zr, Ti)O_3$ films with different crystallographic orientations, Appl. Phys. Lett. **87**, 222903 (2005).
[17] M. Qin, K. Yao, and Y. C. Liang, Photovoltaic mechanisms in ferroelectric thin films with the effects of the electrodes and interfaces, Appl. Phys. Lett. **95**, 022912 (2009).
[18] Z. J. Yue, K. Zhao, S. Q. Zhao, Z. Q. Lu, X. M. Li, H. Ni, and A. J. Wang, Thickness-dependent photovoltaic effects in miscut Nb-doped $SrTiO_3$ single crystals, J. Phys. D **43**, 015104 (2010).
[19] G. L. Yuan and J. L. Wang, Evidences for the depletion region induced by the polarization of ferroelectric semiconductors, Appl. Phys. Lett. **95**, 252904 (2009).
[20] L. Pintilie, V. Stancu, E. Vasile, and I. Pintilie, About the complex relation between short-circuit photocurrent, imprint and polarization in ferroelectric thin films, J. Appl. Phys. **107**, 114111 (2010).
[21] D. W. Cao, H. Zhang, L. A. Fang, W. Dong, F. G. Zheng, and M. R. Shen, Interface layer thickness effect on the photocurrent of Pt sandwiched polycrystalline ferroelectric $Pb(Zr, Ti)O_3$ films, Appl. Phys. Lett. **97**, 102104 (2010).
[22] S. Y. Yang, J. Seidel, S. J. Byrnes, P. Shafer, C. H. Yang, M. D. Rossell, P. Yu, Y. H. Chu, J. F. Scott, J. W. Ager, L. W. Martin, and R. Ramesh, Above-bandgap voltages from ferroelectric photovoltaic devices, Nat. Nanotechnol. **5**, 143 (2010).
[23] W. Ji, K. Yao, and Y. C. Liang, Bulk photovoltaic effect at visible wavelength in epitaxial ferroelectric $BiFeO_3$ thin films, Adv. Mater. **22**, 1763 (2010).
[24] Marin Alexe and Dietrich Hesse, Tip-enhanced photovoltaic effects in bismuth ferrite, Nat. Commun. **2**, 256 (2011).
[25] T. Choi, S. Lee, Y. J. Choi, V. Kiryukhin, and S.-W. Cheong, Switchable ferroelectric diode and photovoltaic effect in $BiFeO_3$, Science **324**, 63 (2009).
[26] R. Nechache, C. Harnagea, S. Licoccia, E. Traversa, A. Ruediger, A. Pignolet, and F. Rosei, Photovoltaic properties of Bi_2FeCrO_6 epitaxial thin films, Appl. Phys. Lett. **98**, 202902 (2011).
[27] Rajesh K. Katiyar, Pankaj Misra, Frank Mendoza, Gerardo Morell, and Ram S. Katiyar, Switchable photovoltaic effect in bilayer graphene/$BiFeO_3$/Pt heterostructures, Appl. Phys. Lett. **105**, 142902 (2014).
[28] Liang Fang, Lu You, Yang Zhou, Peng Ren, Zhi Shiuh Lim, and Junling Wang, Switchable photovoltaic response from polarization modulated interfaces in $BiFeO_3$ thin films, Appl. Phys. Lett. **104**, 142903 (2014).
[29] Seiji Nakashima, Tomohisa Uchida, Daichi Nakayama, Hironori Fujisawa, Masafumi Kobune, and Masaru Shimizu, Bulk photovoltaic effect in a $BiFeO_3$ thin film on a $SrTiO_3$ substrate, Jpn. J. Appl. Phys. **53**, 09PA16 (2014).
[30] Surbhi Gupta, Rohit Medwal, Tej B. Limbu, Rajesh K. Katiyar, Shojan P. Pavunny, Monika Tomar, G. Morell, Vinay Gupta, and R. S. Katiyar, Graphene/semiconductor

silicon modified $BiFeO_3$/indium tin oxide ferroelectric photovoltaic device for transparent self-powered windows, Appl. Phys. Lett. **107**, 062902 (2015).

[31] Rong Li Gao, Chun Lin Fu, Wei Cai, Gang Chen, Xiao Ling Deng, Huai Wen Yang, Ji Rong Sun, and Bao Gen Shen, Enhancement of oxygen vacancies induced photovoltaic effects in $Bi_{0.9}La_{0.1}FeO_3$ thin films, Mater. Sci. Forum **815**, 176 (2015).

[32] R. Nechache, C. Harnagea, S. Li, L. Cardenas, W. Huang, J. Chakrabartty, and F. Rosei, Bandgap tuning of multiferroic oxide solar cells, Nat. Photonics **9**, 61 (2014).

[33] Steve M. Young and Andrew M. Rappe, First Principles Calculation of the Shift Current Photovoltaic Effect in Ferroelectrics, Phys. Rev. Lett. **109**, 116601 (2012).

[34] Steve M. Young, Fan Zheng, and Andrew M. Rappe, First-Principles Calculation of the Bulk Photovoltaic Effect in Bismuth Ferrite, Phys. Rev. Lett. **109**, 236601 (2012).

[35] Lai Jiang, Ilya Grinberg, Fenggong Wang, Steve M. Young, Peter K. Davies, and Andrew M. Rappe, Semiconducting ferroelectric perovskites with intermediate bands via *B*-site Bi^{5+} doping, Phys. Rev. B **90**, 075153 (2014).

[36] John A. Brehm, Steve M. Young, Fan Zheng, and Andrew M. Rappe, First-principles calculation of the bulk photovoltaic effect in the polar compounds $LiAsS_2$, $LiAsSe_2$, and $NaAsSe_2$, J. Chem. Phys. **141**, 204704 (2014).

[37] Fenggong Wang and Andrew M. Rappe, First-principles calculation of the bulk photovoltaic effect in $KNbO_3$ and $(K, Ba)(Ni, Nb)O_{3-\delta}$, Phys. Rev. B **91**, 165124 (2015).

[38] J. E. Sipe and A. I. Shkrebtii, Second-order optical response in semiconductors, Phys. Rev. B **61**, 5337 (2000).

[39] Akash Bhatnagar, Ayan Roy Chaudhuri, Young Heon Kim, Dietrich Hesse, and Marin Alexe, Role of domain walls in the abnormal photovoltaic effect in $BiFeO_3$, Nat. Commun. **4**, 2835 (2013).

[40] A. M. Rappe, K. M. Rabe, E. Kaxiras, and J. D. Joannopoulos, Optimized pseudopotentials, Phys. Rev. B **41**, 1227 (R) (1990).

[41] N. J. Ramer and A. M. Rappe, Designed nonlocal pseudopotentials for enhanced transferability, Phys. Rev. B **59**, 12471 (1999).

[42] X. F. Hao, A. Stroppa, S. Picozzi, A. Filippetti, and C. Franchini, Exceptionally large room-temperature ferroelectric polarization in the $PbNiO_3$ multiferroic nickelate: First-principles study, Phys. Rev. B **86**, 014116 (2012).

[43] P. Giannozzi, S. Baroni, N. Bonini, M. Calandra, R. Car, C. Cavazzoni, D. Ceresoli, G. L. Chiarotti, M. Cococcioni, I. Dabo, A. Dal Corso, S. de Gironcoli, S. Fabris, G. Fratesi, R. Gebauer, U. Gerstmann, C. Gougoussis, A. Kokalj, M. Lazzeri, L. Martin-Samos, N. Marzari, F. Mauri, R. Mazzarello, S. Paolini, A. Pasquarello, L. Paulatto, C. Sbraccia, S. Scandolo, G. Sclauzero, A. P. Seitsonen, A. Smogunov, P. Umari, and R. M. Wentzcovitch, Quantum ESPRESSO: A modular and open-source software project for quantum simulations of materials, J. Phys. Condens. Matter **21**, 395502 (2009).

[44] Jochen Heyd, Gustavo E. Scuseria, and Matthias Ernzerhof, Hybrid functionals based on a screened Coulomb potential, J. Chem. Phys. **118**, 8207 (2003).

[45] Zachary H. Levine and Douglas C. Allan, Linear Optical Response in Silicon and Germanium Including Self-Energy Effects, Phys. Rev. Lett. **63**, 1719 (1989).

[46] F. Nastos, B. Olejnik, K. Schwarz, and J. E. Sipe, Scissors implementation within length-gauge formulations of the frequency-dependent nonlinear optical response of semiconductors, Phys. Rev. B **72**, 045223 (2005).

[47] Yasunobu Inoue, Photocatalytic water splitting by RuO_2-loaded metal oxides and nitrides with d^0- and d^{10}-related electronic configurations, Energy Environ. Sci. **2**, 364 (2009).

[48] L. G. Reznik, A. A. Anikiev, B. S. Umarov, and J. F. Scott, Studies of optical damage in lithium niobate in the presence of thermal gradients, Ferroelectrics **64**, 215 (1985).

[49] A. Anikiev, L. G. Reznik, B. S. Umarov, and J. F. Scott, Perturbed polariton spectra in optically damaged $LiNbO_3$, Ferroelectr. Lett. Sect. **3**, 89 (1985).

[50] Ajay Dhar and Abhai Mansingh, Optical properties of reduced lithium niobate single crystals, J. Appl. Phys. **68**, 5804 (1990).

[51] G. Catalan and J. F. Scott, Physics and applications of bismuth ferrite, Adv. Mater. **21**, 2463 (2009).

[52] J. F. Ihlefeld, N. J. Podraza, Z. K. Liu, R. C. Rai, X. Xu, T. Heeg, Y. B. Chen, J. Li, R. W. Collins, J. L. Musfeldt, X. Q. Pan, J. Schubert, R. Ramesh, and D. G. Schlom, Optical band gap of $BiFeO_3$ grown by molecular-beam epitaxy, Appl. Phys. Lett. **92**, 142908 (2008).

[53] J. Seidel, D. Y. Fu, S. Y. Yang, E. Alarcon-Llado, J. Q. Wu, R. Ramesh, and J. W. Ager, Efficient Photovoltaic Current Generation at Ferroelectric Domain Walls, Phys. Rev. Lett. **107**, 126805 (2011).

[54] W. Ji, K. Yao, and Y. C. Liang, Evidence of bulk photovoltaic effect and large tensor coefficient in ferroelectric $BiFeO_3$ thin films, Phys. Rev. B **84**, 094115 (2011).

[55] K. Momma and F. Izumi, VESTA: A three-dimensional visualization system for electronic and structural analysis, J. Appl. Crystallogr. **41**, 653 (2008).

[56] Yoshiyuki Inaguma, Kie Tanaka, Takeshi Tsuchiya, Daisuke Mori, Tetsuhiro Katsumata, Tomonori Ohba, Ko-ichi Hiraki, Toshihiro Takahashi, and Hiroyuki Saitoh, Synthesis, structural transformation, thermal stability, valence state, and magnetic and electronic properties of $PbNiO_3$ with perovskite- and $LiNbO_3$-type structures, J. Am. Chem. Soc. **133**, 16920 (2011).

[57] K. A. Rabe, M. Dawber, C. Lichtensteiger, C. H. Ahn, and J. M. Triscone, Modern physics of ferroelectrics: Essential background, Top. Appl. Phys. **105**, 1 (2007).

[58] J. B. Neaton, C. Ederer, U. V. Waghmare, N. A. Spaldin, and K. M. Rabe, First-principles study of spontaneous polarization in multiferroic $BiFeO_3$, Phys. Rev. B **71**, 014113 (2005).

[59] Sergey V. Levchenko and Andrew M. Rappe, Influence of Ferroelectric Polarization on the Equilibrium Stoichiometry of Lithium Niobate (0001) Surfaces, Phys. Rev. Lett. **100**, 256101 (2008).

[60] Christoph Baeumer, Diomedes Saldana-Greco, John Mark P. Martirez, Andrew M. Rappe, Moonsub Shim, and Lane W. Martin, Ferroelectrically driven spatial carrier density modulation in graphene, Nat. Commun. **6**, 6136 (2015).

[61] X. F. Hao, A. Stroppa, P. Barone, A. Filippetti, C. Franchini, and S. Picozzi, Structural and ferroelectric transitions in magnetic nickelate $PbNiO_3$, New J. Phys. **16**, 015030 (2014).

[62] A. W. Sleight and C. T. Prewitt, High-pressure $HgTiO_3$ and $HgPbO_3$: Preparation, characterization, and structure, J. Solid State Chem. **6**, 509 (1973).

[63] Yoshiyuki Inaguma, Masashi Yoshida, and Tetsuhiro Katsumata, A polar oxide $ZnSnO_3$ with a $LiNbO_3$-type structure, J. Am. Chem. Soc. **130**, 6704 (2008).

[64] Huiyang Gou, Faming Gao, and Jingwu Zhang, Structural identification, electronic and optical properties of $ZnSnO_3$: First principle calculations, Comput. Mater. Sci. **49**, 552 (2010).

[65] Takahiro Takei, Rie Haramoto, Qiang Dong, Nobuhiro Kumada, Yoshinori Yonesaki, Nobukazu Kinomura, Takayuki Mano, Shunsuke Nishimoto, Yoshikazu Kameshima, and Michihiro Miyake, Photocatalytic activities of various pentavalent bismuthates under visible light irradiation, J. Solid State Chem. **184**, 2017 (2011).

[66] Tarun K. Bera, Joon I. Jang, Jung-Hwan Song, Christos D. Malliakas, Arthur J. Freeman, John B. Ketterson, and Mercouri G. Kanatzidis, Soluble semiconductors $AAsSe_2$ (A = Li, Na) with a direct-band-gap and strong second harmonic generation: A combined experimental and theoretical study, J. Am. Chem. Soc. **132**, 3484 (2010).